Pergamon

Int. J. Heat Mass Transfer. Vol. 38, No. 8, pp. 1409–1425, 1995

0017-9310/95 $9.50+0.00

0017-9310(94)00250-9

Boiling flow through a rod-bundle channel: steady states and dynamic instabilities

K. WHITFIELD and R. P. ROY†

Arizona State University, Department of Mechanical and Aerospace Engineering, Tempe, AZ 85287-6106, U.S.A.

(*Received* 23 *March* 1994 *and in final form* 28 *July* 1994)

Abstract—Steady state and dynamic instability experiments were performed at low mass velocities in a Refrigerant-113 boiling flow rig featuring a vertical electrically heated 16 rod-bundle channel. The important nondimensional parameters associated with a typical 64-rod boiling water nuclear reactor fuel assembly were matched with the exception of the Froude number. Measurements at steady states include the transverse distributions of vapor fraction and fluid temperature at two axial locations along the rod-bundle channel. The evolution of dynamic instability in the channel was studied by examining the energy spectrum of the inlet flow rate variation. The instabilities were found to be of the quasiperiodic oscillation kind. A limited parametric study of the highest energy oscillation state was carried out.

INTRODUCTION

The cooling fluid in nuclear reactor cores and steam generators typically flows axially through a rod-bundle configuration. Flow boiling takes place, its extent being a function of the rate of thermal energy input, fluid flow rate, pressure, and subcooling. Depending on the operating condition, the flow may be stable or unstable. For safe and efficient operation, it is necessary to understand both the steady state and dynamic characteristics of the coolant flow.

In the present work, which is primarily experimental, attention was given to boiling flow at low mass velocity through a vertical electrically heated 16 rod-bundle channel. The objective was to investigate the flow at mass velocities comparable to natural circulation flow through a boiling water nuclear reactor (BWR) fuel assembly operating at low power. An experimental rig with Refrigerant-113 as the working fluid was designed by scaling the important system parameters so as to provide a good simulation, at much lower pressure and temperature, of the thermal-hydraulic state in a BWR fuel assembly.

A survey of literature indicates that earlier studies of boiling flow in rod-bundle channels essentially fall into three categories. The first two categories deal with, respectively, the steady state and dynamic instability characteristics of the flow in a purely thermal-hydraulic sense. The third category, which studies flow in BWR core, also addresses neutronic coupling.

The purely thermal-hydraulic studies, *ca* 1969 and 1979, respectively, were reviewed by Lahey and Schraub [1] and Rowe [2]. Computational codes have been developed for simulation of boiling flow through rod-bundle configurations, for example refs. [3, 4]. One of the earliest experimental studies of the frequency response of boiling flow through a rod-bundle channel was by Nylund *et al.* [5]. A significant study of the dynamic stability of high-pressure boiling water flow through a 19-heater rod-bundle channel was reported by Collins and Gacesa [6]. Carver [7] analyzed the effect of a parallel bypass flow on the stability of flow through a rod-bundle channel. Blomstrand *et al.* [8] and Nylund *et al.* [9] conducted experiments at forced and natural circulation conditions on the flow stability of a new BWR fuel assembly design. The fuel assembly was simulated by 64 electrically heated rods arranged in an 8×8 configuration in a square channel with partitions.

Dynamic stability tests have been performed in several operating BWRs, for example refs. [10–12]. Some of these tests were run at rather extreme conditions (high power-to-flow ratios) and limit cycle oscillations were observed. Analysis of dynamic instability of BWRs have also been carried out, for example refs. [13, 14].

THE EXPERIMENTS

Scaling criteria

The coolant in a BWR core is water at high pressure and temperature. To simulate the thermal and fluid mechanical condition of this coolant at sufficiently reduced pressure, temperature, and input power suitable for laboratory experiments, fluid-to-fluid scaling [15, 16] was carried out. Refrigerant-113 (R-113) was found to be an appropriate fluid. Scaling involved the matching of the following nondimensional groups for geometric and physical similarity:

Density ratio,

$$N_{\mathrm{d}} \equiv \frac{\rho_{\mathrm{G}}}{\rho_{\mathrm{L}}}$$

scales the system pressure

† Author to whom correspondence should be addressed.

NOMENCLATURE

$A_{X\text{-}S}$ flow area of channel
D_h rod-bundle channel hydraulic diameter, defined in eq. (1)
f friction factor
g acceleration due to gravity
G mass velocity of fluid
h_f saturation enthalpy of liquid
h_{fg} latent heat of vaporization
h_L liquid enthalpy
K_i, K_e inlet, exit throttling (orifice) coefficients, $\equiv (\Delta p_{i(or\,e)}/\frac{1}{2}\rho U_{L,in}^2)$
L_H heated length of channel
p pressure
P_h heated perimeter
P_w wetted perimeter
$\dot{Q}$ total input heating power
$\dot{q}'''$ input heating power per unit volume of fluid in channel
s rod-bundle pitch
T_G, T_L vapor, liquid mean temperature
u mean axial fluid velocity
U_G mean axial vapor velocity
U_L mean axial liquid velocity
v_f specific volume of saturated liquid.

Greek symbols
$\langle\alpha\rangle$ line- or area-average vapor fraction at an axial location in the channel
ρ_L, ρ_G liquid, vapor density
σ surface tension
Δp, $\overline{\Delta p}$ pressure drop, mean pressure drop.

Subscripts
in channel inlet
fluid vapor–liquid mixture.

Equilibrium phase change number,

$$N_{pch} \equiv \frac{\dot{q}''' L_H (\rho_L - \rho_G)}{\rho_L u_{in} h_{fg} \rho_G}$$

a measure of the power-to-flow ratio

Subcooling number,

$$N_{sub} \equiv \frac{(h_f - h_{L,in})(\rho_L - \rho_G)}{h_{fg}\rho_G}$$

scales the inlet subcooling

Froude number,

$$N_{Fr} \equiv \frac{u_0^2}{g L_H}$$

indicates the relative importance of inertia and gravity where u_0, a velocity scale,

$$= \frac{\dot{q}''_w P_h v_f L_H}{A_{x-s}(h_f - h_{L,in})} \quad [17]$$

Weber number,

$$N_{We} \equiv \frac{\rho_L \sigma}{G^2 D_h}$$

scales surface tension effect

Friction number,

$$\Lambda \equiv \frac{f L_H}{2 D_h}$$

depends on flow geometry and regime

Orifice numbers,

$$N_{orf,i}, N_{orf,e} \equiv \text{function}\,(K_i \text{ or } K_e)$$

channel inlet and exit flow restrictions

Axial-to-lateral scale factor, $\equiv L_H/D_h$

In a square-lattice rod-bundle channel (Fig. 2), accounting for the channel wetted walls, the hydraulic diameter is

$$D_h \equiv \frac{4 \cdot (\text{flow area})}{\text{wetted perimeter}} = \frac{d_{rod}\left[\frac{4}{\pi}(s/d_{rod})^2 - 1\right]}{[1 + s/(\pi d_{rod})]}. \quad (1)$$

Apart from the definition given in the nomenclature, the Froude number may be defined as (u_{in}^2/gL_H), where u_{in} is the fluid velocity at the channel inlet. The former definition has the same qualitative dependence on u_{in} as seen in the following:

$$N_{Fr} \equiv \frac{u_0^2}{gL_H} = \left[\frac{\dot{Q}_{in}}{\rho A_{X\text{-}S}(h_f - h_{L_{in}})}\right]^2 \frac{1}{gL_H} \quad (2)$$

where $\dot{Q}_{in}$ is the total input power at a particular thermal-hydraulic condition in the rod-bundle channel. Now, for a fixed inlet subcooling, $\dot{Q}_{in}$ is proportional to u_{in}. Therefore, from equation (2)

$$N_{Fr} \sim \frac{u_{in}^2}{gL_H} \quad (3)$$

It was decided at the very outset to adopt a full-length 16-heater rod-bundle channel with a flow area equal to one-fourth of a typical 64-rod BWR fuel assembly [18]. An advantage of this choice over a scaled-down channel is that the spacing between the adjacent rods is sufficiently large to traverse various probes for measurements in the fluid. A disadvantage is that it becomes difficult to match the Froude number. As will be discussed later, the Froude number may have a significant influence on the dynamic behavior of boiling flow.

Values of the thermal-hydraulic scaling parameters for a BWR fuel assembly at natural circulation con-

Table 1. Values of nondimensional scaling parameters and some dimensional quantities

	BWR-6 (natural circulation condition)	R-113 experimental rig
L_H	3.66 m	3.66 m
D_h	0.0123 m	0.0123 m
Pressure	6.62 MPa	0.89 MPa
N_d (at saturation state)	0.046	0.047
N_{sub}	1.2–1.4	>1
N_{pch}	8–9	$\lesssim 9$
N_{We}	0.004–0.006	0.005–0.01
N_{Fr}	0.15	$\lesssim 0.005$
K_i	60†	$\gtrsim 70$‡
K_e	2–3§	$\gtrsim 5$‖

† Inlet orifice and lower tie plate.
‡ Includes inlet piping.
§ Upper tie plate.
‖ Includes exit valve and some piping.

dition and the R-113 experimental rig are given in Table 1.

Experimental rig

Figure 1 is a schematic diagram of the experimental rig. The main components of the rig are: the rod-bundle channel, the bypass line, the flow mixer, the centrifugal pump, the main heat exchanger, the after-cooler, and a regulated d.c. power supply. As stated earlier, R-113 was the working fluid.

The rod-bundle channel is shown schematically in Fig. 2. This channel is comprised of an inlet plenum, the heated length and the exit plenum. Three 1.22 m long, 6.76 cm × 6.76 cm inner dimension, 4.8 mm wall stainless steel square channels with flanged ends are connected in series to form the outer shell of the heated length. The shell houses 16 heater rods arranged in a 4 × 4 square lattice. Each rod contains a coiled nichrome heater element (resistance = $0.425 \pm 0.004\ \Omega$) embedded in magnesium oxide insulation and encased in a 1.22 cm o.d., 0.84 mm wall incoloy sheath. At each end of the heater rod, a copper rod 0.64 cm in diameter serves as the carrier of electric current to or from the nichrome element. Seven ferrule-type stainless steel spacers maintain the transverse positions of the heater rods along the channel while allowing the fluid to flow through. To minimize heat loss, the entire rod-bundle channel is insulated with jacketed fiberglass wool.

A flexible stainless steel bellows located just upstream of the rod-bundle channel isolates the channel to some extent from pump-induced vibration and permits thermal expansion of the channel. Flow throttling at the channel inlet is provided by a 3.81 cm globe valve. Exit throttling is provided via a 5.08 cm ball valve located just downstream of the exit plenum.

Two locations, junctions 1 and 2, are marked in Fig. 1. These denote, respectively, the beginning and the end of the *rod-bundle channel flow path*. This path is parallel to an 8.3 cm i.d. unheated bypass line. The bypass line carries a much higher flow rate (greater by a factor of 10 or more) than the rod-bundle channel during the dynamic instability experiments. The objective of this is to impose a pressure drop across the rod-bundle channel flow path which, ideally, would be constant, in which case the configuration of one channel in parallel with many channels is simulated. The bypass flow is controlled by a butterfly valve.

Flow exiting the rod-bundle channel joins the bypass flow in the mixer. While the former flow is usually of a vapor–liquid mixture, the latter is of subcooled liquid. As such, condensation occurs in the flow mixer. The internal design of the mixer has been found to be very important. This is because the rod-bundle channel flow dynamics can be affected by the processes within the mixer. We tested two mixer designs. In the first design, the flow from the rod-bundle channel discharged into the bypass flow through an open-ended 6.35 cm diameter pipe which extended into the mixer. This gave rise to a pressure oscillation of 0.8–0.9 Hz frequency in the mixer (possibly due to a condensation instability) and caused flow to oscillate at the same frequency in the rod-bundle channel. This was unacceptable and so a second design was introduced. In this design, the flow from the rod-bundle channel discharged into the mixer through 400 holes of 3.2 mm diameter around a 6.35 cm diameter pipe with closed end. Use of this mixer eliminated the 0.8–0.9 Hz oscillation and the dynamics of the rod-bundle channel flow could now be studied. One other precautionary measure was taken to ensure that the dynamics of the flow mixer was effectively isolated from that of the rod-bundle channel—the flow restriction, K_e, at the channel exit was maintained above 100. This of course, meant that all of our instability experiments were to be conducted at relatively high exit throttling.†

The flow from the mixer is directed to the heat

† Results of some past works indicate however that the influence of K_e on the instability of channel flow is not as strong as that of K_i [19, 20].

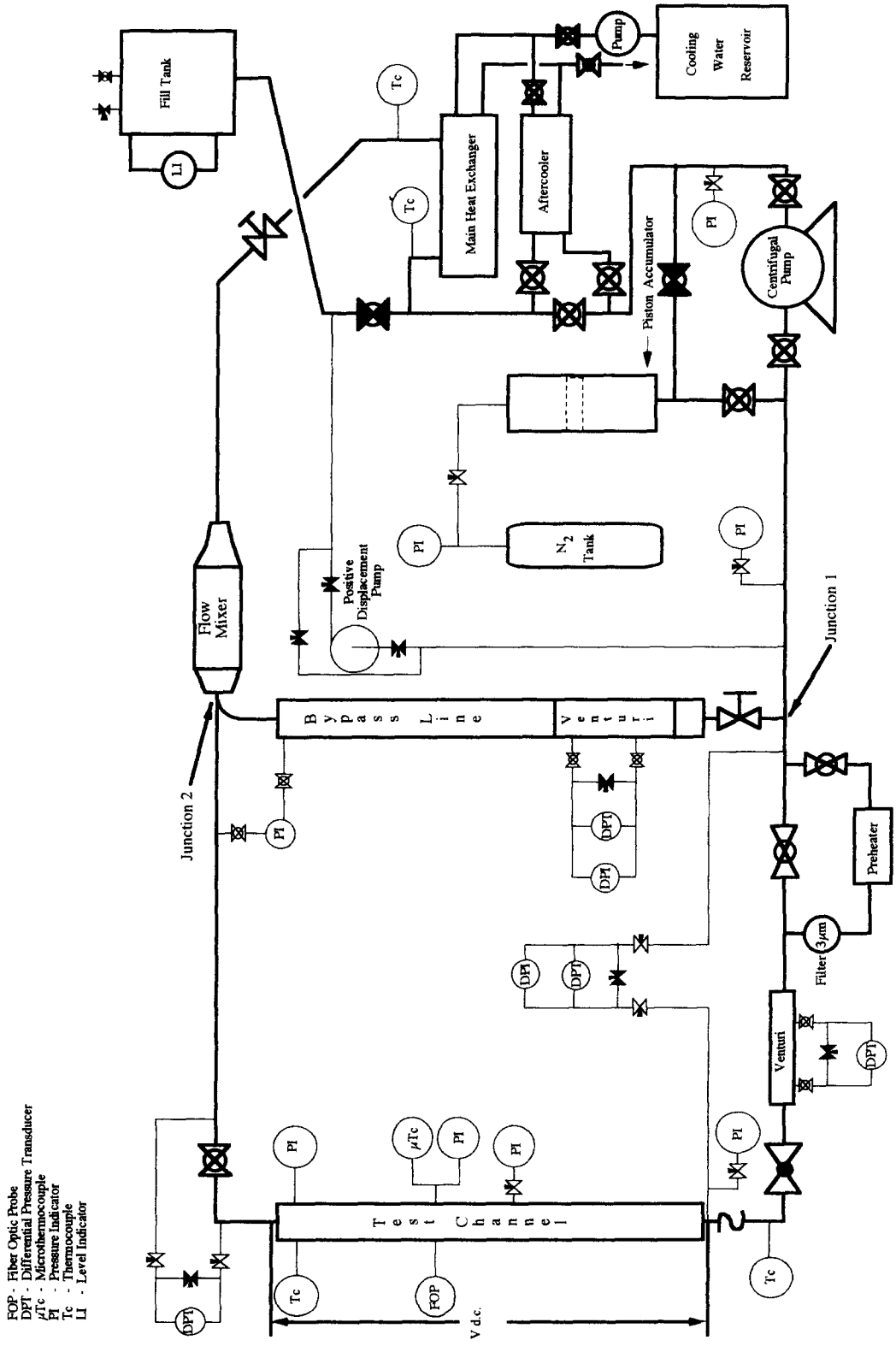

Fig. 1. The experimental rig.

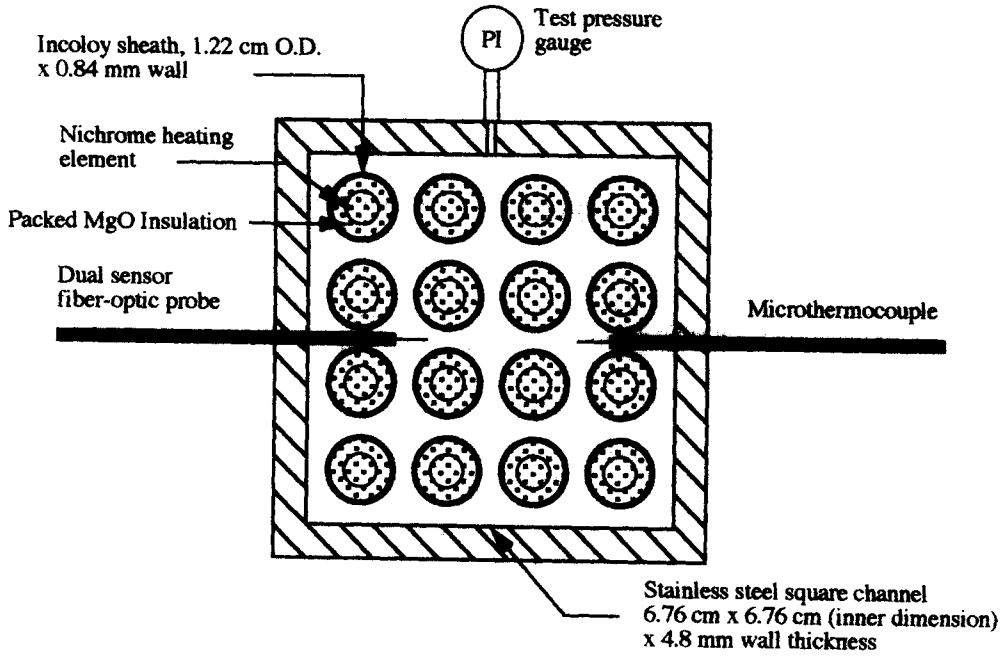

(a) Cross-sectional view at m.p. 2

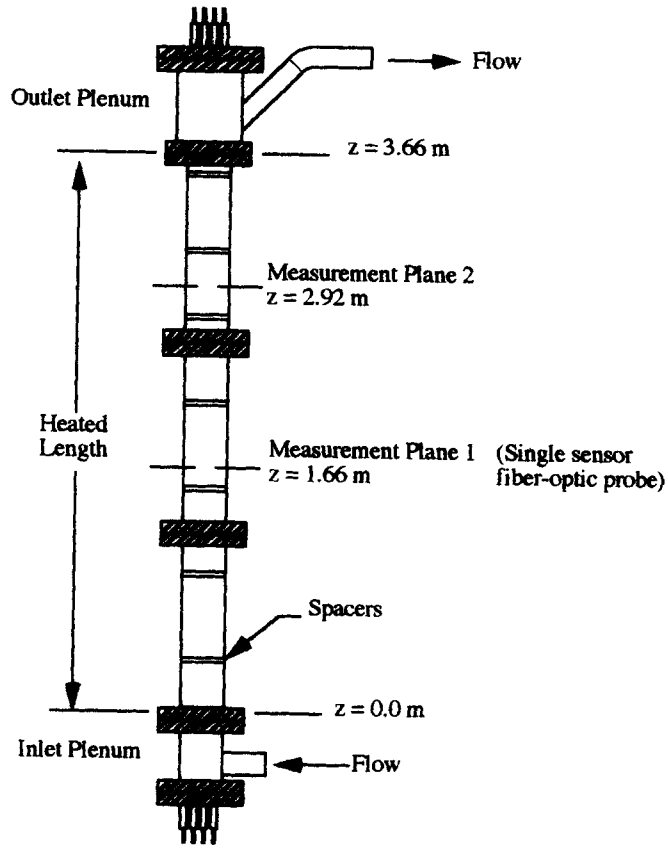

(b) Elevation view

Fig. 2. The rod-bundle channel.

exchangers. The main heat exchanger, a four-pass shell-and-tube unit with 3.81 m^2 heat transfer area provides most of the heat removal. The two-pass shell-and-tube aftercooler with a heat transfer area of 0.85 m^2 is used, when necessary, for fine adjustment of fluid temperature.

A stainless steel centrifugal pump (Ingersol-Rand) supplies R-113 at up to a maximum rate of 10.1 liters s^{-1} at 284 kPa head. A piston accumulator connected to the pump discharge pipe pressurizes the system and provides some fluid expansion volume (the rest is provided by the fill tank). The accumulator is isolated from the system during the instability experiments since the presence of such a compressible volume may affect the dynamics of the rod-bundle channel flow.

Power to the heater rods is supplied from a regulated d.c. supply (Rapid Power Technologies) rated at 60 kW (40 V, 1500 A).

Measurement instrumentation

The following were monitored continuously during all experiments: (i) the rod-bundle channel inlet flow rate, (ii) fluid temperature and pressure at channel inlet and exit; also pressure at an intermediate axial location, (iii) input power to the heater rods and (iv) the bypass flow rate.

The channel inlet flow rate was measured by a venturi-differential pressure transducer (DPT) combination. The DPT signal was routed to a data acquisition and analysis system (DATA 6000A, Analogic) and to a digital oscilloscope (Nicolet 2090) where the temporal behavior of the signal was tracked. The bypass flow rate was also measured by a venturi–DPT combination. Copper–constantan thermocouples (with stainless steel sheath) measured the fluid temperatures at the channel inlet and exit. Bourdon tube test pressure gages measured the channel pressures. The power input to the heater rods was determined from the measured total current flow through the 16 rods and the average voltage drop across them.

The pressure drops across the rod-bundle channel inlet piping and globe valve and the exit ball valve ($\sim K_i$ and K_e, respectively) were measured by DPTs.

Measurements in the fluid were performed at two axial locations in the rod-bundle channel, measurement plane (m.p.)1 and m.p.2 (Fig. 2). A single-sensor fiber-optic probe (FOP) was installed at m.p.1. This probe (Photonetics, France) measures the local vapor residence time fraction (henceforth called vapor fraction). The FOP probe is described briefly in ref. [21]. m.p.2 in the channel was instrumented with a dual-sensor FOP and a fast-response chromel–alumel microthermocouple [22]. In addition to local vapor fraction measurement, the dual-sensor FOP is capable of measuring vapor bubble axial velocity and bubble size [21]. The time constants of the FOP sensor and the microthermocouple were about 10 μs and 3.4 ms, respectively. It is possible to distinguish between vapor and liquid temperatures in significantly subcooled boiling flow by means of the microthermocouple [22].

During the steady state experiments, the FOPs and the microthermocouple were traversed to obtain the transverse distributions of the respective measurands.

Experimental procedure

Air is highly soluble in R-113. As such, the rig fluid was carefully degassed before each experiment. Then, the remaining dissolved air was measured by an Aire-Ometer (Seaton–Wilson). This was always small enough so that its effects on the R-113 pressure, saturation temperature, and vapor fraction were minimal.

Heat balance tests were performed with steady flow of single-phase liquid through the rod-bundle channel. These tests indicated that less than 1% of the total power supplied to the 16 heater rods was lost to the ambient. Measurement of the liquid temperature at the channel inlet, m.p.2, and channel exit also showed that the heat flux distribution along the heater rods (in a 16-rod average sense) was not uniform but, rather, slightly skewed to higher heat flux toward the top. This was taken into account when calculating the thermal hydraulic condition in the channel for each steady state experiment.

The procedure for the steady state experiments was straightforward and will not be described here. As for the instability experiments, the following were established at the very outset of each with flow of single-phase liquid: the nominal flow rates through the rod-bundle channel and the bypass line, the channel inlet pressure, and the channel inlet and exit throttling coefficients. The bypass flow rate/channel flow rate ratio was maintained between 12 and 13. Such a ratio is generally considered to be large enough to invoke a constant pressure drop boundary condition across the channel, for example refs. [6, 7]. However, this was not quite the case in our experiments as will be explained later.

Each instability experiment proceeded via small quasistatic increments of power to the rod-bundle. Commencement of significant boiling in the channel caused a small decrease in the nominal channel flow rate. The flow rate continued to decrease slightly as the extent of boiling increased with power addition. At selected conditions during the evolution of flow instability, time series records of the rod-bundle channel inlet flow signal and the bypass flow signal (typically, 16 384 samples at 25 ms interval yielding a 6.8 min long record for each) were acquired. These records were subsequently analyzed and the energy spectra of the flow rate variations obtained. The frequency resolution of these spectra is estimated to be 0.04 Hz and the possible calculation error in the energy density up to 25%.

RESULTS AND DISCUSSION

Steady state experiments

Table 2 shows the ranges of rod-bundle channel variables and the associated measurement uncer-

Table 2. Range of steady state experiments and measurement uncertainties† (rod-bundle channel)

	Range	Uncertainty
Mass velocity [kg m^{-2} s^{-1}]	238–319	±2
Inlet pressure [kPa]	750–905	±2
Inlet temperature [°C]	94–107	±0.2
Total power input [kW]	22–33	±0.05

† The uncertainty estimates are for 95% confidence.

tainties for these experiments. To ensure stable flow, high inlet throttling ($K_i \approx 400$) was provided.

Of the six experiments performed, the nominal conditions for experiments 1–3 were as given in Table 3. These three experiments correspond to, respectively, low, moderate and high vapor fraction at m.p.2. The results of experiments 1 and 3 are presented here in more detail. Brief comments are also made on experiment 2.

Figure 3(a)–(d) shows the measurements at m.p.2 for steady state experiment 1. Figure 3(a) is a plot of the vapor fraction distribution along a center line of the rod-bundle channel from the channel wall vicinity to its center. The locations of the heater rods along the FOP traverse are shown schematically as shaded semicircles. A wave-like variation of vapor fraction along the center line is seen, the crests being at or near the smallest inter-rod gaps.

At this experimental condition, the flow regime at m.p.2 is expected to be bubbly. Figure 3(b) shows the distribution of the mean axial velocity of vapor bubbles along the same traverse. The variation of velocity essentially follows that of the vapor fraction.

Figure 3(c) is a plot of the fluid (i.e. vapor–liquid mixture) temperature distribution along the same center line, but now from the opposite wall of the channel to its center. The distribution is close to uniform although a slight waviness can be observed with the crests at about the same locations as the vapor fraction crests. The temperatures are quite close to the local saturation temperature of the fluid. It was not possible to separate the vapor and liquid temperatures by statistical tools such as the probability density function (PDF) because the temperatures of the two phases were too close to each other (although the liquid was probably slightly subcooled).

Figure 3(d) shows the PDF of the vapor bubble diameter (assuming that the bubbles are spherical) at a location 27.8 mm from the channel wall. This size distribution was obtained by a statistical technique from the measured bubble chord length distribution [21]. The highly peaked shape of the PDF is appropriate for bubbly flow regime. The most probable bubble diameter is about 0.7 mm. The bubble sphericity assumption lends some uncertainty to this result.

No vapor was detected at m.p.1 by the single-sensor probe in this experiment.

Figure 4(a)–(d) shows the measurements at m.p.2 for steady state experiment 3. Data are presented in these figures in the same sequence as the previous experiment. Figure 4(a) indicates that in the wave-like distribution of vapor fraction along the channel center line, the crests have shifted to the *central subchannel* regions (each of these regions is surrounded by four rods in a square lattice). The vapor axial velocity variation follows that of vapor fraction. The fluid temperature distribution is again essentially uniform. The bubble diameter PDF [Fig. 4(d)] is much flatter. It appears that the larger vapor bubbles have migrated to the central subchannels. Also, a transition to the churn-turbulent flow region is possibly underway. An eventual transition to the annular flow regime can be expected in the central subchannels at higher vapor fractions.

Measurements at m.p.2 for the moderate vapor fraction ($\approx$25%) experiment 2 showed that the crests in the wavy distribution of vapor fraction remain at or near the smallest inter-rod gap regions (similar to experiment 1). The bubble diameter PDF also remained highly peaked, this being consistent with bubbly regime expected at m.p.2 for this experimental condition. The bubbles were, however, generally larger in comparison to experiment 1.

The steady state measurements were compared with the results of a one-dimensional two-fluid model simulation of the flow through a central subchannel of the rod-bundle channel (Fig. 5). The model equations and solution method have been reported in refs. [19, 23]. In the calculation, provision for increased wetted perimeter due to the channel walls was made in accordance with equation (1). The area-average fluid temperature at any axial location is calculated from the area-average liquid and vapor temperatures as follows:

$$\langle T_{\text{fluid}} \rangle = \langle \alpha \rangle \langle T_G \rangle + \langle 1-\alpha \rangle \langle T_L \rangle. \quad (4)$$

For comparison purpose, the "measured" mean liquid axial velocity is calculated from the measured mean vapor axial velocity by the relation

$$\langle U_L \rangle = \langle U_G \rangle - U_{\text{relative}} \quad (5)$$

where, for bubbly flow regime, from ref. [24]

Table 3. Steady state experiments 1–3

	Experiment 1	Experiment 2	Experiment 3
Mass velocity [kg m^{-2} s^{-1}]	239	319	315
Inlet pressure [kPa]	905	753	753
Inlet temperature [°C]	94.1	104.5	106.2
	(N_{sub} = 7.36)	(N_{sub} = 4.49)	(N_{sub} = 4.12)
Total power input [kW]	31.45	22.00	22.55

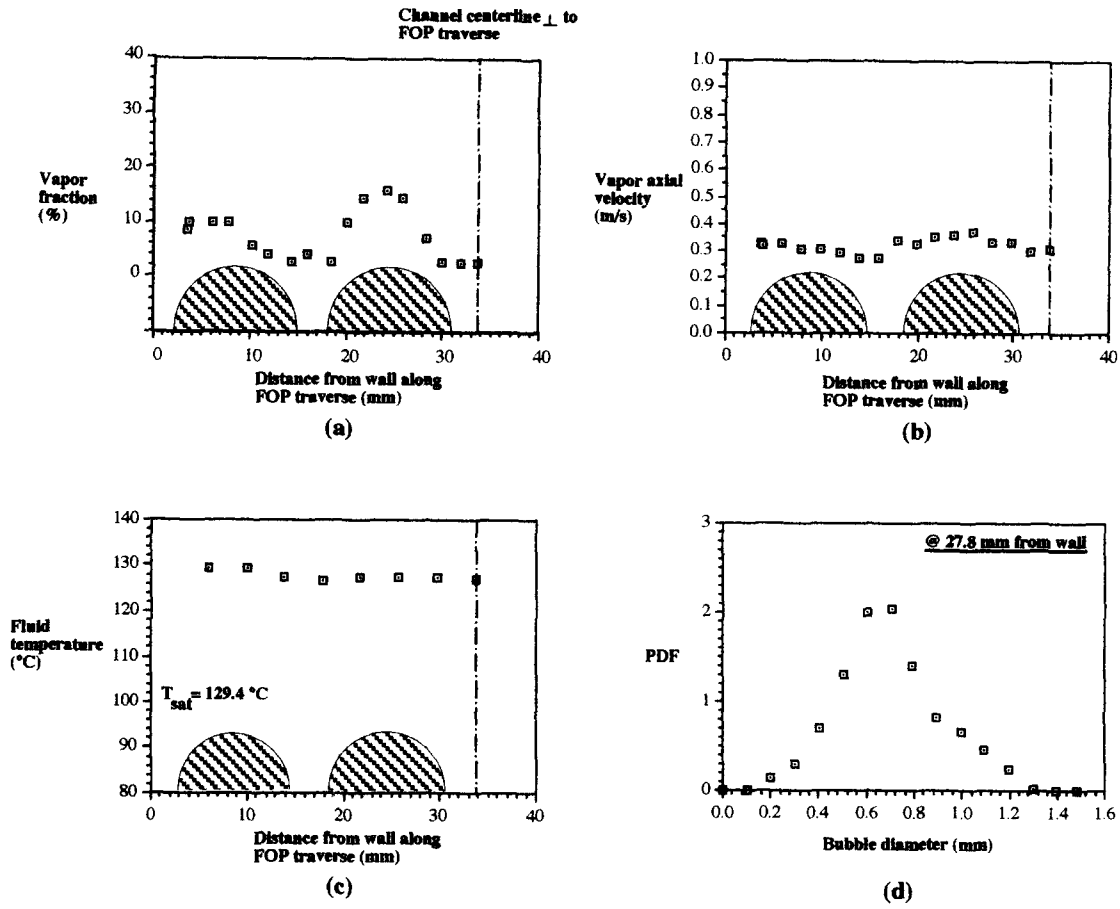

Fig. 3. Steady state experiment 1: measurements at m.p.2.

$$U_{\text{relative}} = 1.53\left[\frac{\sigma g(\rho_L - \rho_G)}{\rho_L^2}\right]^{1/4}(1-\langle\alpha\rangle)^{1/2}. \quad (6)$$

Table 4 shows a comparison of the measured (chord-average along center line) and calculated (area-average) values of some variables at m.p.2 for steady state experiment 1. The agreement is quite good. However, the approximate nature of the model equations and the uncertainties associated with the measurements must be kept in mind during such comparisons.

Figure 5 contains the calculated area-average vapor fraction profiles along the rod-bundle channel for steady state experiments 1–3. The measured chord-average vapor fractions at m.p.1 (this is zero in all three experiments) and m.p.2 are also shown. The agreement is good.

Dynamic instability experiments

Table 5 lists the ranges of nominal values of rod-bundle channel variables spanned by these experiments and the corresponding measurement uncertainties.

A total of 32 instability experiments were performed. Of these, nine were with the first flow mixer design and were rejected because, as stated earlier, the internal dynamics of the flow mixer acted as the driver of the rod-bundle flow dynamics. Of the remaining 23 experiments, all of which were run with the second flow mixer, 11 were found to be in regions of

Table 4. Measured and calculated values of some variables at m.p.2: steady state experiment 1

	Measured	Calculated
Vapor fraction [%]	7.4	8.4
Fluid temperature [°C]	128.9	128.8
Pressure [kPa]	863	867
Vapor axial velocity [m s^{-1}]	0.32	0.32
Liquid axial velocity [m s^{-1}]	0.19	0.20

Table 5. Ranges of dynamic instability experiments and measurement uncertainties† (rod-bundle channel)

	Range (nominal)	Uncertainty
Mass velocity [kg m^{-2} s^{-1}]	332–383	±2
Inlet pressure [kPa]	750–857	±2
Inlet temperature [°C]	104–114	±0.2
Total input power [kW]	$\lesssim$34	±0.05
Inlet throttling coefficient, K_i	68–186	±2
Exit throttling coefficient, K_e	128–132	±2

† The uncertainty estimates are for 95% confidence.

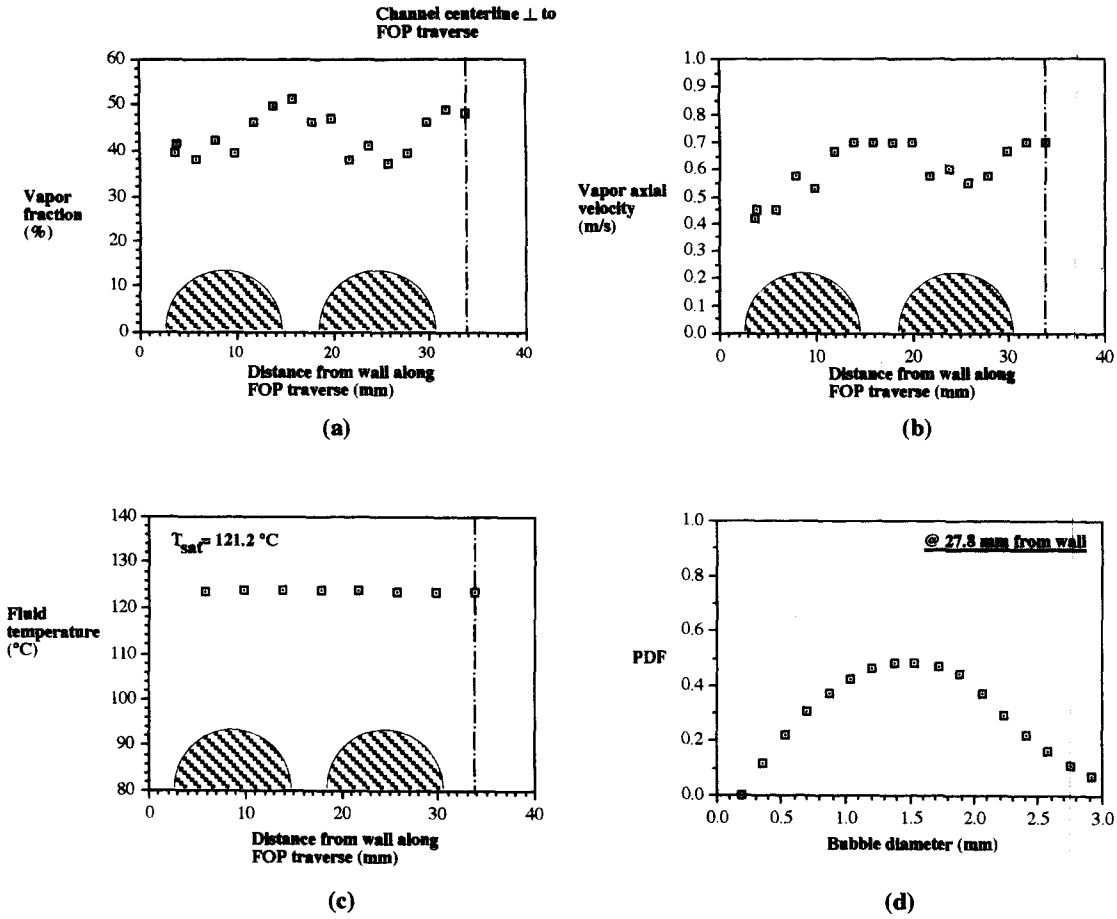

Fig. 4. Steady state experiment 3 : measurements at m.p.2.

Table 6. Nominal conditions for instability experiments 1–3

	Experiment 1	Experiment 2	Experiment 3
Mass velocity [kg m^{-2} s^{-1}]†	397–360	399–361	400–365
Inlet pressure [kPa]	822	822	787
Inlet temperature [°C]	108.1 (N_{sub} = 4.30)	110.2 (N_{sub} = 3.87)	106.2 (N_{sub} = 4.42)
Inlet throttling coefficient, K_i	70	70	108
Exit throttling coefficient, K_e	129	131	130
Bypass flow rate/channel flow rate	≈12	≈12	≈12.5

† As stated earlier, the nominal flow rate through the channel decreased monotonically as more power was supplied during these experiments.

$N_{sub}-N_{pch}-N_{Fr}$ space where only weak (i.e. low energy) dynamic instabilities developed.† The remaining 12 experiments culminated in relatively strong (i.e. high energy) dynamic instabilities. The results of three of these (experiments 1–3) are presented here in some detail. The other nine are included in a discussion of parametric effects.

The channel nominal experimental conditions for experiments 1–3, other than the input power, were as shown in Table 6.

Experiment 2 differs from experiment 1 in the inlet temperature and thus in N_{sub}. Experiment 3 differs from experiment 1 primarily in K_i.

Figure 6(a)–(d) shows, for instability experiment 1, the energy spectra of the rod-bundle channel inlet flow rate variation at four stages during the evolution of instability. These stages are at successively higher input powers. In each spectrum, the prevailing values of N_{pch}, N_{Fr}^{-1}, and the rms value of inlet flow rate variation (in l/min) are given.

Although only four spectra are shown, seven were obtained at successively higher input powers. Scrutiny of the spectra reveals four distinct stages in the development of the flow instability. Figure 6(a) cor-

† In most of these experiments, N_{sub} was less than 3.

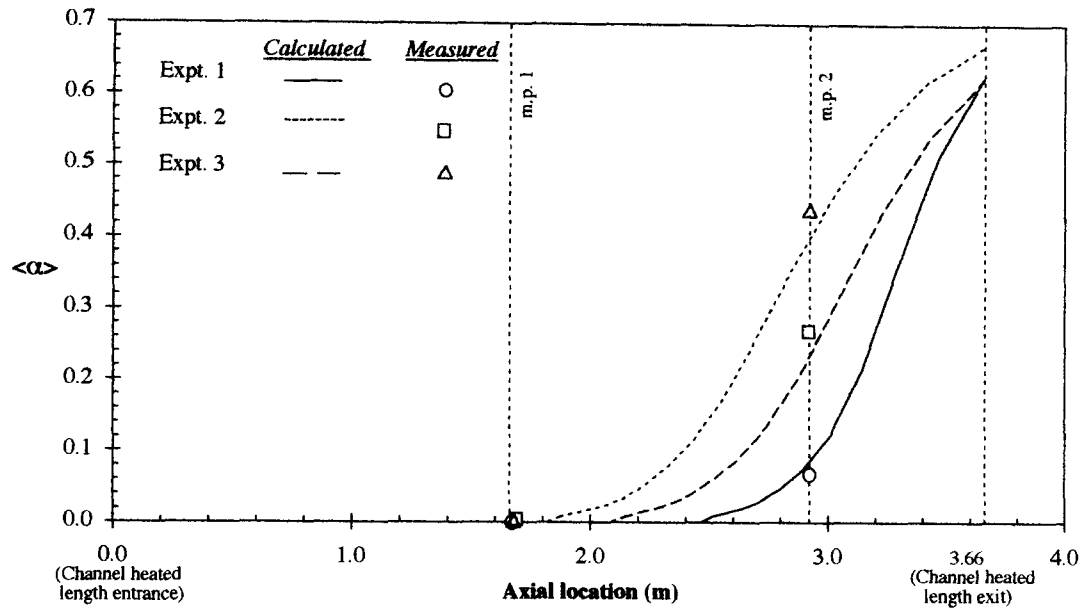

Fig. 5. Vapor fraction profiles along the rod-bundle channel for steady state experiments 1–3.

responds to the first stage. Here, significant boiling had just commenced at m.p.2 (as detected by the FOP). Boiling had, of course, begun at the channel exit earlier. A peak at an identifiable frequency with a distribution around it characterizes the spectrum. Examination of the inlet flow trace indicates that the flow variation was not truly periodic. This feature along with the limited frequency resolution and accuracy of the spectrum suggest the presence of more than one frequency in the instability.† The appearance of a dominant peak in the spectrum points to an important change in the nature of the flow because such a feature was not present at nonboiling (but heated) conditions. Also, while the inlet flow variation (oscillation) energy was still modest, its value had gradually increased to about four times the value for nonboiling flow. It may be suggested that a supercritical Hopf bifurcation from an unstable fixed point took place when boiling commenced in the channel and a quasiperiodic flow oscillation began. It is interesting to note that a small-amplitude flow oscillation was reported by Collins and Gacesa [6] soon after significant boiling occurred in their rod-bundle channel.

As more power was supplied to the rod-bundle, the flow oscillation energy increased and one or more additional peaks of lower energy content appeared [Fig. 6(b) and (c)]. The dominant peak frequency remained about the same, (a)–(c). The additional peak frequencies in (b) and (c) were not commensurate with the dominant peak frequency. This suggests secondary Hopf bifurcations and continued quasiperiodic flow oscillation. This is the second stage in the development of instability.

At a still higher power input, the ancillary peaks became inconspicuous while the dominant peak with a distribution around it remained (the peak frequency was now slightly higher than at the first stage) [Fig. 6(d)]. This was also the condition where the flow oscillation was the most energetic. The time trace of the flow signal again indicated that the flow oscillation was quasiperiodic. This is the third stage in the development of the instability. Further power increases resulted in gradual reduction of the flow oscillation energy as well as additional bifurcations to multiple incommensurate peak frequencies. A dominant peak remained. This is the fourth stage.

We designate the rod-bundle channel condition at the third stage as the highest energy quasiperiodic flow oscillation (HEQFO) state. It is a state that could possibly be used to study the effects of various parameters on the instability development.

Figure 7 shows the time traces of the channel inlet venturi pressure drop oscillation and the exit valve pressure drop oscillation at the HEQFO state. Both are normalized as

$$\frac{\Delta p(t)-\overline{\Delta p}}{\overline{\Delta p}}.$$

The time-average value of the pressure drop across the exit valve was significantly larger than that of the inlet venturi pressure drop.‡ This is not only because K_e was larger than K_i but also due to high vapor fraction at the exit. The two pressure drop oscillations appear to be roughly 180 degrees out of phase.§ Explanation of this phase difference in terms of vapor frac-

† This was confirmed later by performing a chirp-z-transform of the signal whcih yielded better frequency resolution over a preselected frequency range (for example 0–1.2 Hz).

‡ This, of course, can not be seen in Fig. 9 because of the normalization.

§ This phase difference estimate is based only on visual inspection of the two signals.

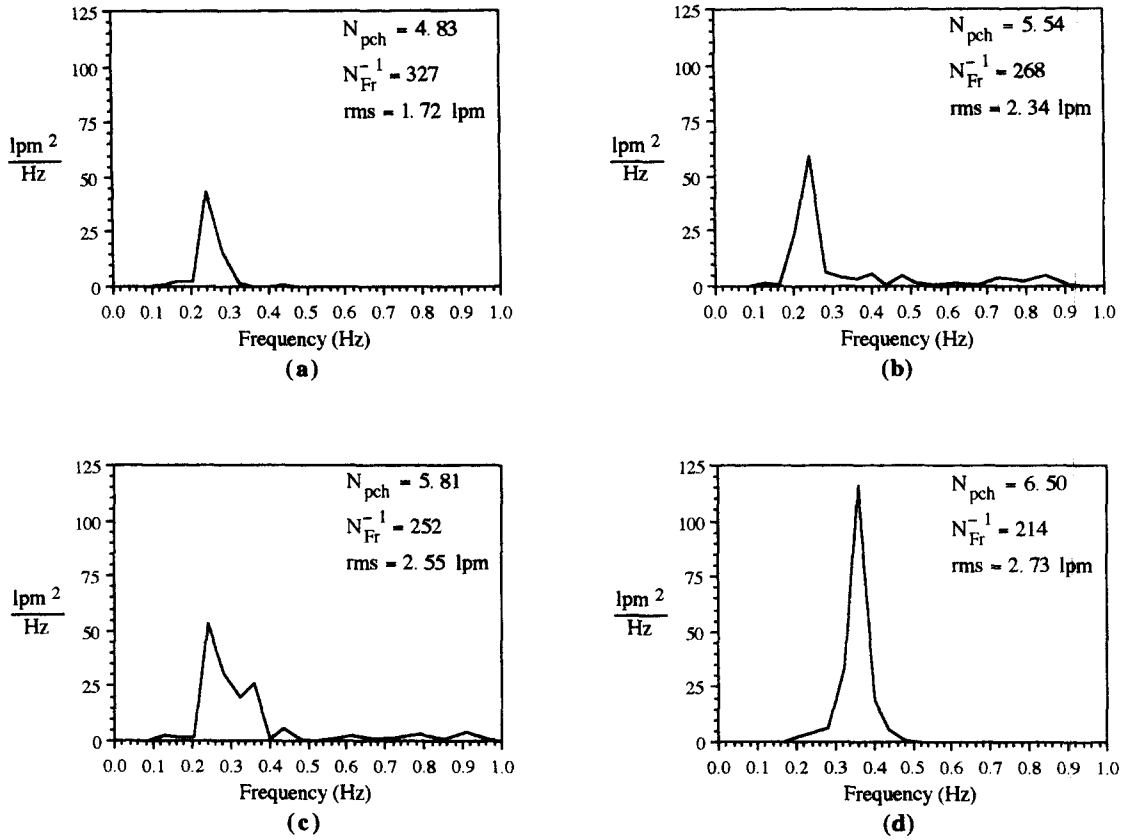

Fig. 6. Dynamic instability experiment 1 : energy spectra of flow rate variation at rod-bundle channel inlet.

tion (void) waves propagating from the channel inlet to its exit has been suggested by researchers, for example refs. [25, 26]. While this is plausible, complicating factors can be present in experiments rendering such an explanation less clearcut. An example of such complications in our experiment is the temporal variation of the bypass flow and thus of the pressure drop imposed across the rod-bundle channel flow path.

The bypass flow rate–channel flow rate ratio was about 12 for this experiment. Examination of the bypass flow signal indicated that this flow also experienced a quasiperiodic oscillation with about the same absolute energy content as the channel flow, Fig. 8. The rms value of the bypass flow oscillation as a percent of the mean bypass flow rate was, of course, an order of magnitude smaller than that for the channel flow. Also, the bypass flow oscillation was roughly 180° out of phase with the flow oscillation at the channel inlet and approximately in phase with the exit valve pressure drop oscillation. The bypass flow oscillation was thus essentially in phase with the flow oscillation at the channel exit. Similar observations were reported in [6].

The flow mixer very possibly played a major role in the temporal behavior of the pressure at junction 2 (Fig. 1). Experimental rigs such as the present one must, therefore, pay careful attention to the design of the mixer and the dynamics of the processes within it.

Figure 9(a)–(d) contains the energy spectra of the channel inlet flow oscillation for instability experiment 2. Figure 9(d) shows the energy spectrum for the HEQFO state. This state was not as distinctly apart in this experiment as in experiment 1. The phase relationships between the channel inlet flow, exit flow, and bypass flow were similar to those in experiment 1.

Figure 10(a)–(d) presents the rod-bundle channel inlet flow variation spectra for instability experiment 3. Figure 10(d) shows the HEQFO state. As mentioned earlier, this experiment featured a larger inlet throttling the influence of which is discussed later.

Some general observations regarding the instabilities are now in order. Firstly, we note that the boiling flow system is a nonlinear dynamical system. It is also noisy, the noise arising from the pump, the flow mixer and other rig components. It is important in a study such as this to minimize noise. It is also important that extraneous dynamic modes be eliminated so that they do not excite the system, e.g. through the boundary conditions [27]. The flow mixer, which establishes the hydrodynamic boundary condition at the rod-bundle channel flow path exit, is important from both of these perspectives.

Secondly, two nondimensional parameters, namely

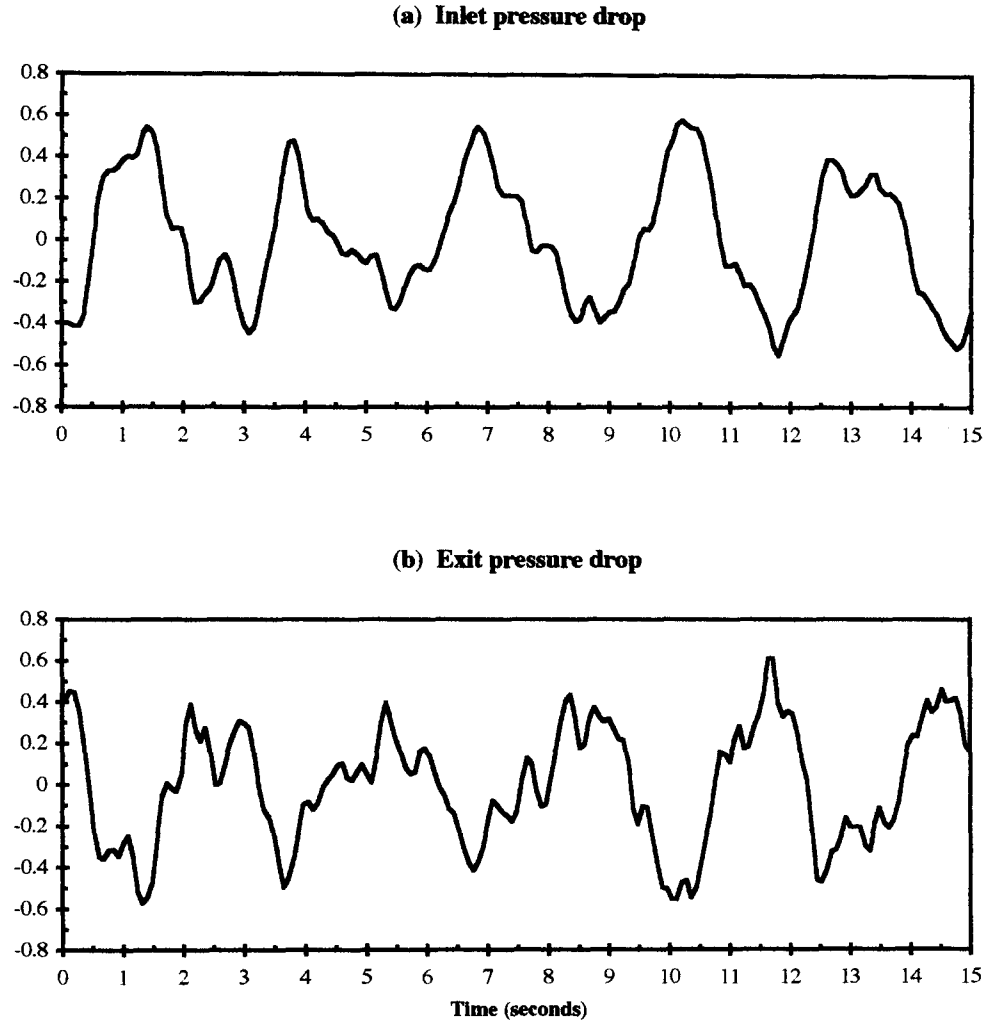

Fig. 7. Normalized inlet venturi and exit valve pressure drop oscillations at the HEQFO state: instability experiment 1.

N_{pch} and N_{Fr}, underwent changes as the instability evolved in these experiments. This is a more complicated scenario than one in which only one parameter varies at any one time (this is the case in many theoretical studies).

Thirdly, it should be noted that N_{Fr}^{-1} was always greater than 200 during the experiments, meaning that the channel mass velocity was always low and gravitational effect significant. It has been pointed out that boiling flow systems may exhibit chaotic behavior under such a circumstance [28]. The mass velocities in our experiments appear to have been high enough that instead of chaotic oscillations the flow exhibited a behavior intermediate between periodic and chaotic†, namely quasiperiodic. The energy spectra contained one or more significant peaks with distributions around them as well as low-amplitude noise. Supercritical Hopf bifurcations, including secondary ones, are suggested as the mechanism of evolution of the instabilities.

Fourthly, examination of the channel inlet flow rate time record shows the feature of intermittency. Intermittency describes oscillations that are periodic for some time intervals with aperiodic oscillations in between [30]. If, in response to the variation of system parameter(s), the flow approaches a state of chaotic oscillation, the durations of the aperiodic oscillations increase. The quasiperiodic character of a flow oscillation may coexist with intermittency.

Finally, the only way in which N_{Fr}^{-1} could have been significantly reduced in these experiments is by increasing the flow rate through the rod-bundle channel. This, of course, would have required that the bypass flow rate be increased proportionately. The capacity of the circulating pump was not sufficiently high to accomplish these.

Parametric effects on the HEQFO state. As mentioned earlier, this state was identified by the highest flow oscillation energy content (i.e. an upper bound)

† The energy spectrum of a chaotic oscillation is characterized by a broad-band noise, with or without discrete peaks [29].

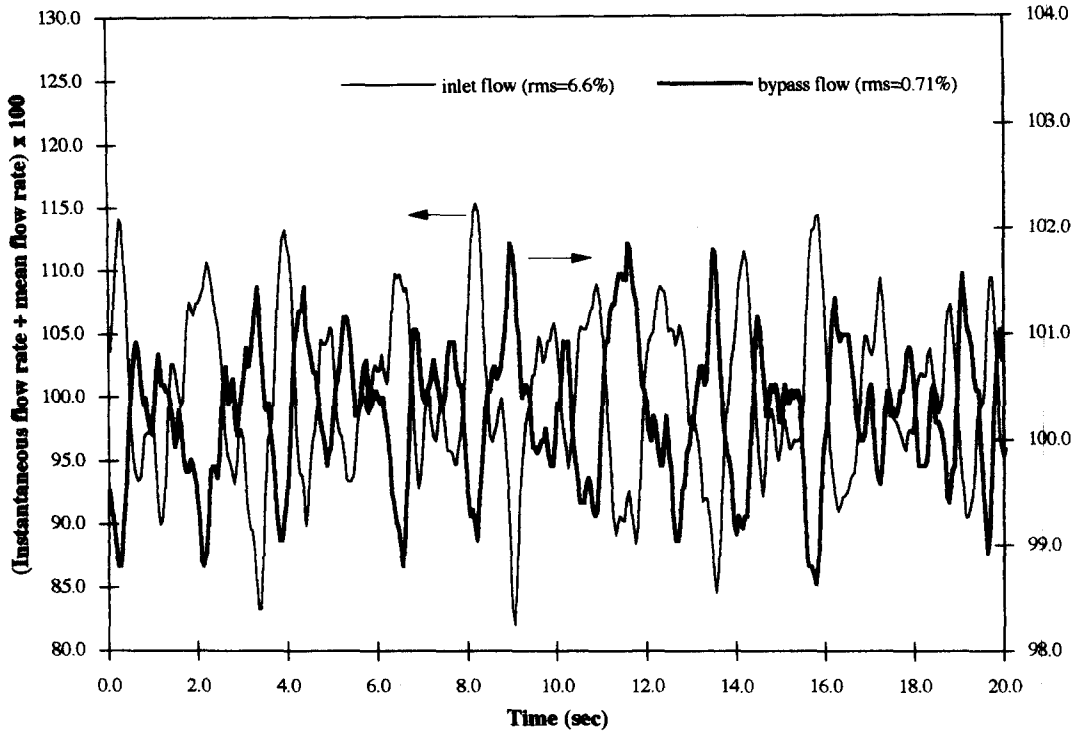

Fig. 8. Channel inlet and bypass flow rate signals.

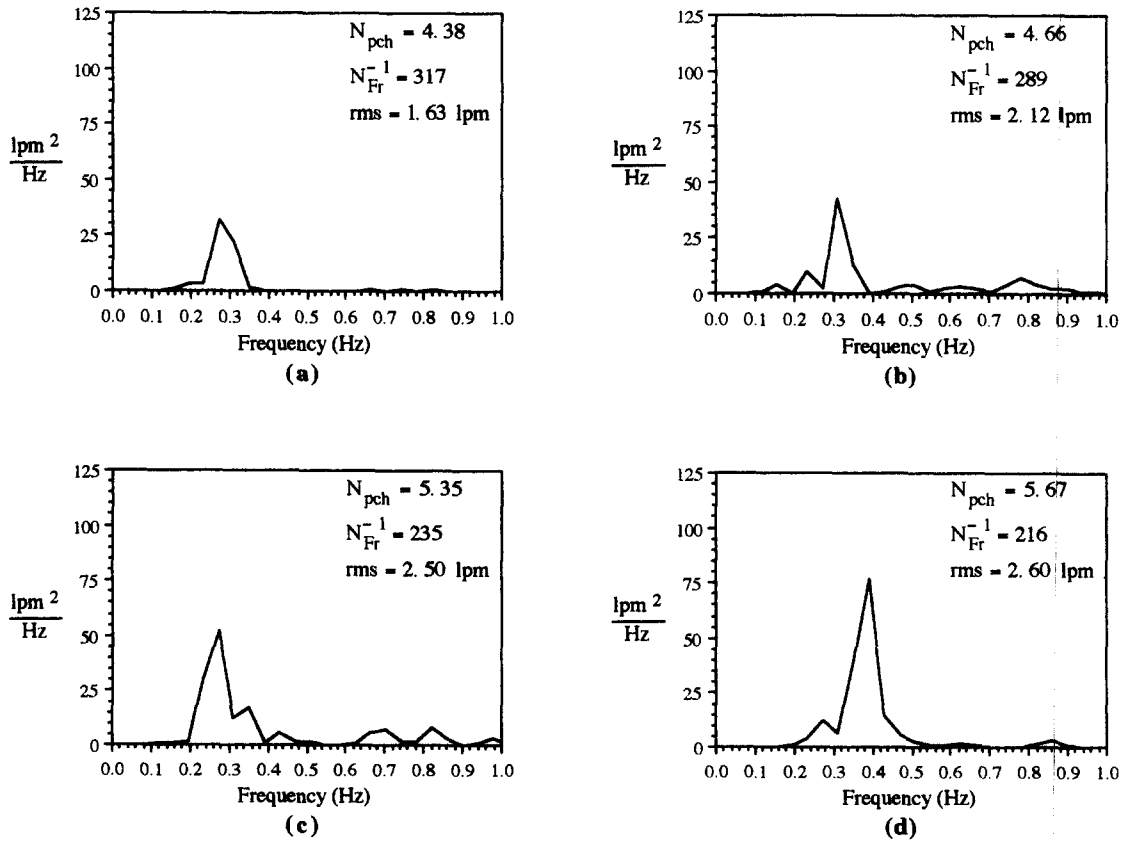

Fig. 9. Dynamic instability experiment 2—energy spectra of flow rate variation at rod-bundle channel inlet.

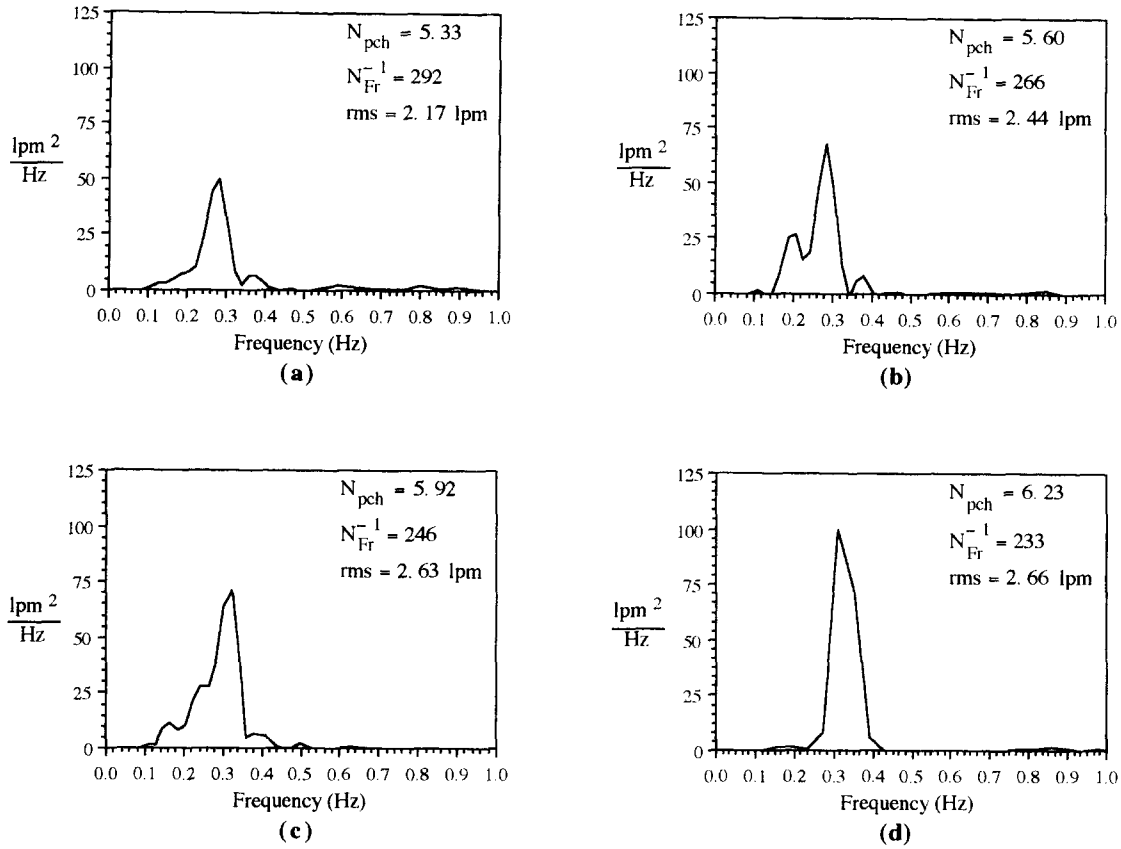

Fig. 10. Dynamic instability experiment 3—energy spectra of flow rate variation at rod-bundle channel inlet.

and, usually, one dominant peak frequency with a distribution around it. It is an important state in the sense that it may determine whether the corresponding operating condition is acceptable from the viewpoint of operational safety (for example flow-induced vibrations, thermal fatigue, precipitation of critical heat flux condition, etc.). An understanding of the nature of the oscillation may also suggest a means of controlling it [27].

In the following, a limited parametric investigation of the HEQFO state is reported. The channel parameters which were varied are: mass velocity, inlet subcooling, inlet throttling coefficient, K_i, and inlet pressure.

The effect of mass velocity on the power input at the HEQFO state is shown in Fig. 11. N_{sub}, K_i and K_e were maintained essentially constant in these experiments although N_{fr}^{-1} necessarily varied. Increase in the mass velocity resulted in an increase in the required power. A mass velocity increase also led to an increase in the dominant peak frequency value (Fig. 12).

The range of N_{sub} examined in our study is rather narrow, $\approx$3.2–4.4. This is mainly because we wished to maintain N_{sub} above 3. As mentioned earlier, below N_{sub} of 3, the instability appeared to weaken considerably and it became difficult to identify the HEQFO state unambiguously. In Fig. 13, we show the effect of N_{sub} on the input power at the HEQFO state. N_{Fr}^{-1} was maintained within a reasonably close range in these experiments. The required power input increased with N_{sub}.

Increasing the inlet throttling coefficient, K_i, has been found to be stabilizing in studies of marginal stability boundary. In our experiments, since the inception of instability more or less coincided with the commencement of boiling in the rod-bundle channel, K_i had no detectable effect on instability inception. One discernible effect of a higher K_i was a reduction in the inlet flow oscillation energy throughout the evolution of the instability. Figure 14 shows flow oscillation energy at the HEQFO state for four values of K_i. Thus, K_i still had a beneficial influence since it attentuated the oscillation. One other effect was observed at the two experiments with high inlet throttling (K_i = 143, 186). The channel inlet flow oscillation became more coherent in that the ancillary low energy peaks in the spectra mostly disappeared. The oscillation remained quasiperiodic however.

Four experiments were performed to observe the influence of inlet pressure on the input power at the HEQFO state. In these, the mass velocity, N_{sub}, K_i and K_e were maintained approximately same and N_{Fr}^{-1} was maintained within a narrow range. The input power was found to increase with pressure.

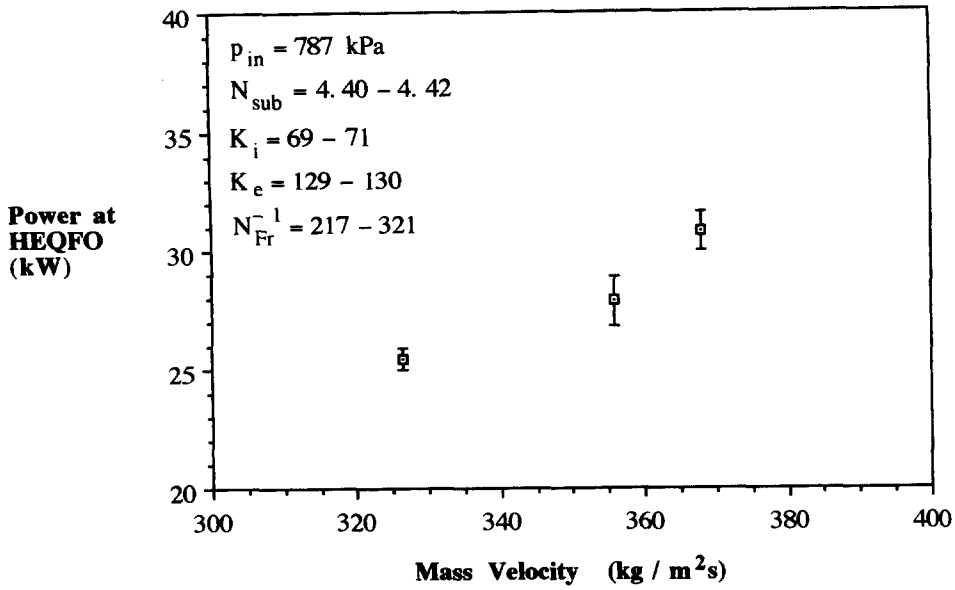

Fig. 11. Effect of channel mass velocity on the input power at HEQFO state.

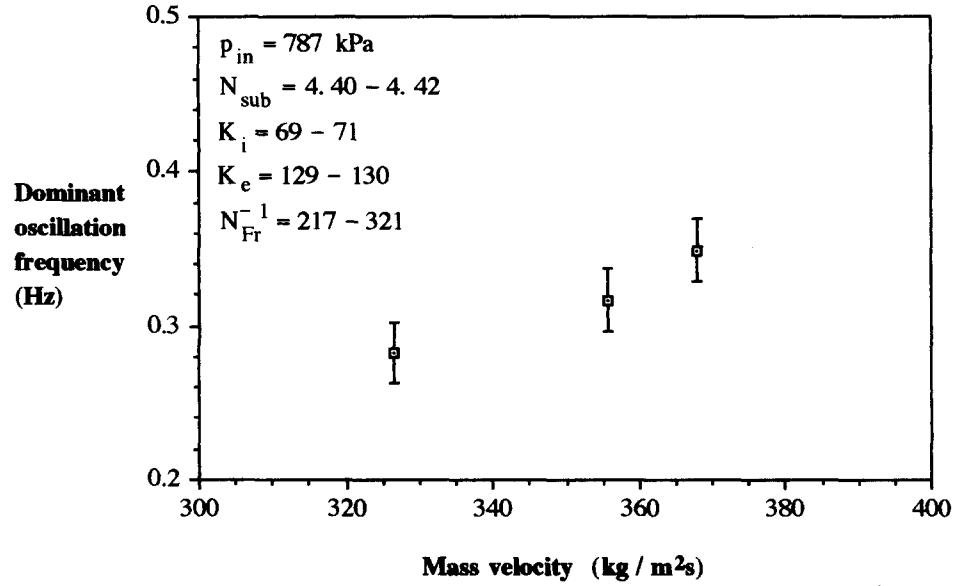

Fig. 12. Effect of channel mass velocity on the dominant flow oscillation frequency peak at HEQFO state.

CONCLUDING REMARKS

The experiments reported here were confined to low mass velocities representative of natural circulation flow through BWR fuel assemblies. In scaling the experimental rig, it was possible to match all important nondimensional parameters with the exception of the Froude number. The Froude number was an order of magnitude smaller in our experiments, primarily because a full-length rod-bundle channel with the same axial-to-lateral geometric scale factor as the fuel assembly was chosen and the circulating pump capacity was not sufficiently high. The lower Froude number meant that the effect of gravity was more pronounced.

The steady state experiments were run with high throttling at the rod-bundle channel inlet, thereby ensuring flow with minimal variation. Vapor fraction distribution measurements showed that the flow regime in the central subchannels began a transition from bubbly to churn-turbulent (with larger vapor bubbles) beyond an average vapor fraction of about 40%. Fluid temperature distribution measurements showed that saturated boiling took place beyond an average vapor fraction of about 10%.

Scrutiny of the time traces and energy spectra of

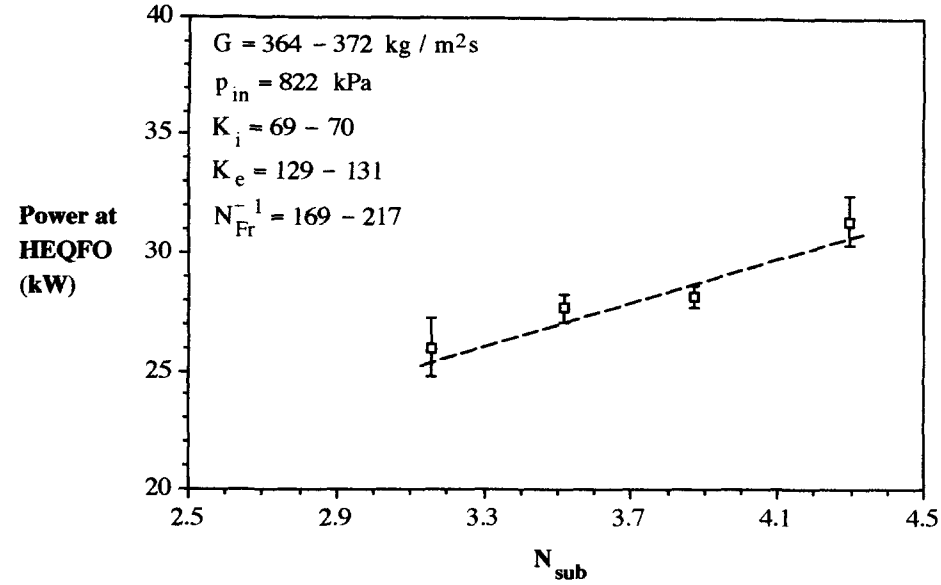

Fig. 13. Effect of channel inlet subcooling on the input power at HEQFO state.

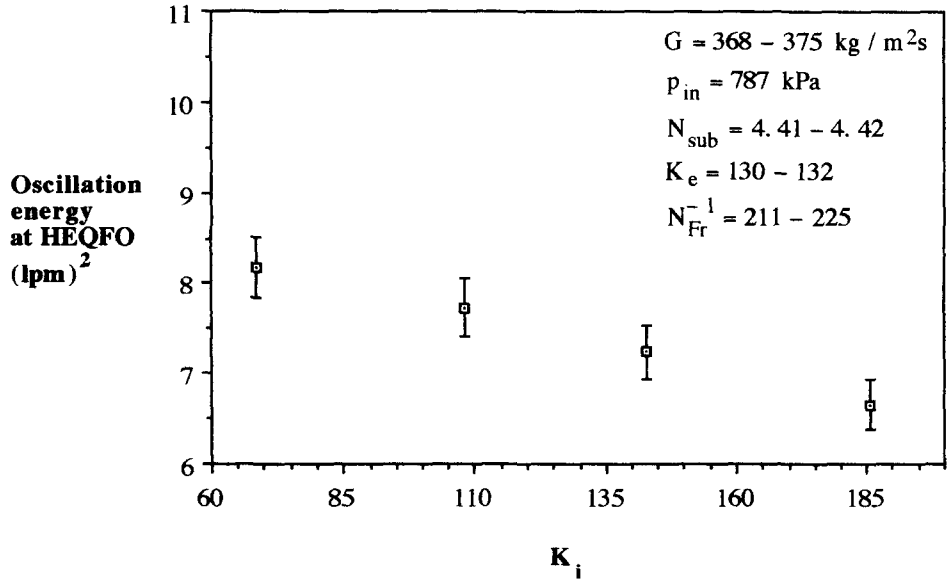

Fig. 14. Effect of inlet throttling on the energy content of channel inlet flow oscillation at HEQFO state.

the channel inlet flow rate signal showed that the instabilities were quasiperiodic and some, in fact, may not have been too far from chaotic. That this is expected at low Froude numbers has been pointed out by other researchers.

Limited experimental resolution and system noise make it more difficult to follow the evolution of instabilities in a physical experiment than in a numerical simulation.

Finally, three areas of improvement are being contemplated for future experiments. Firstly, a larger flow rate through the rod-bundle channel is necessary. This will allow instability experiments at higher Froude numbers. Secondly, a higher bypass flow rate to channel flow rate ratio would be helpful. These two improvements require a larger capacity circulating pump. Finally, further improvement in the flow mixer design is needed. This should result in smaller pressure variations at the channel flow path exit. Measurement of temporal pressure variations at various locations in the flow mixer will be required to ascertain this.

Acknowledgements—This research was funded by General Electric, Nuclear Energy and the Nuclear Regulatory Commission. Helpful discussions with Drs B. Shiralkar and B. Matzner of GE and Dr H. Scott of NRC are gratefully acknowledged.

REFERENCES

1. R. T. Lahey, Jr. and F. A. Schraub, Mixing, flow regimes and void fraction for two-phase flow in rod bundles.

In *Two-Phase Flow and Heat Transfer in Rod-Bundles* (Edited by V. E. Schrock), pp. 1–14. ASME Winter Annual Meeting, Los Angeles (1969).
2. D. S. Rowe, Progress in thermal-hydraulics for rod- and tube-bundle geometries. In *Fluid Flow and Heat Transfer Over Rod or Tube Bundles* (Edited by S. C. Yao and P. A. Pfund) pp. 1–12. ASME Winter Annual Meeting, New York (1979).
3. D. S. Rowe, COBRA-IIIC: a digital computer program for steady-state and transient thermal-hydraulic analysis of rod bundle nuclear fuel elements, Battelle, Pacific Northwest Laboratories, BNWL-1695 (1973).
4. C. W. Stewart *et al.*, VIPRE-01: a thermal-hydraulic analysis code for reactor cores, Battelle, Electric Power Research Institute Report EPRI NP-2511-CCM (1983).
5. O. Nylund *et al.*, *FRIGG Loop Project*. ASEA-Atom, Sweden (1968).
6. D. B. Collins and M. Gacesa, Hydrodynamic instability in a full-scale simulated reactor channel, *Proc. Instn Mech. Engrs*, Paper 15, Vol. 184 (3G) (1969–1970).
7. M. B. Carver, Effect of by-pass characteristics on parallel-channel flow instabilities, *ibid*, Paper 11.
8. J. Blomstrand, L. H. Broddfelt and S. Haque, Stability investigations of SVEA-64 BWR fuel, NURETH-4, *Proceedings of the Fourth International Topical Meeting on Nuclear Reactor Thermal-Hydraulics*, Vol. 1, pp. 560–567 (1989).
9. O. Nylund and C. Jönsson, On the hydrodynamic stability of water-cross BWR fuel assemblies, *Jahrestagnung Kerntechnik*, pp. 113–116 (1990).
10. L. A. Carmichael and R. O. Niemi, Transient and stability tests at Peach Bottom Atomic Power Station unit 2 at the end of cycle 2, Electric Power Research Institute Report EPRI NP-972 (1978).
11. Y. Waaranpera and S. Andersson, BWR stability testing: reaching the limit-cycle threshold at natural circulation, *Trans. Am. Nucl. Soc.* **39,** 868 (1981).
12. S. A. Sandoz and S. F. Chen, Vermont Yankee stability tests during cycle 8, *Trans. Am. Nucl. Soc.*, **45,** 754 (1983).
13. J. M. Sorensen, J. M. Healzer and J. A. Naser, BWR stability calculations with RETRAN, *Proceedings of the International RETRAN Conference*, Las Vegas, EPRI NP-3803-SR (1985).
14. F. Araya, K. Yoshida, M. Hirano and Y. Yabushita, Analysis of a neutron flux oscillation event at LaSalle-2, *Nucl. Technol.* **93,** 82–90 (1991).
15. R. L. Kiang, Scaling criteria for nuclear reactor thermal-hydraulics. In *Basic Aspects of Two-Phase Flow and Heat Transfer*, HTD **34,** 67–74, Twenty-second National Heat Transfer Conference (1984).
16. P. Symolon, Scaling of two-phase flow in a rod bundle with Freon, *Proceedings of the Sixth Conference on Nuclear Thermal Hydraulics*, Washington D.C., American Nuclear Society, pp. 291–302 (1990).
17. J. L. Achard, D. A. Drew and R. T. Lahey, The analysis of density-wave oscillations in boiling channels, *J. Fluid Mech.* **155,** 213–232 (1985).
18. B. S. Shiralkar, GE Nuclear Energy, private communication (1990).
19. R. C. Dykhuizen, R. P. Roy and S. P. Kalra, A linear time-domain two-fluid model analysis of dynamic instability in boiling flow systems, *ASME J. Heat Transfer* **108**(1), 100–108 (1986).
20. D. M. France, R. D. Carlson and R. P. Roy, Measurement and analysis of dynamic instabilities in fluid heated two-phase flow, *Int. J. Heat Mass Transfer* **29**(12), 1919–1929 (1986).
21. R. P. Roy, V. Velidandla, S. P. Kalra and P. Peturaud, Local measurements in the two-phase region of turbulent subcooled boiling flow, *ASME J. Heat Transfer* **116**(3), 660–669 (1994).
22. P. Beckman, R. P. Roy, K. Whitfield and A. Hasan, A fast-response microthermocouple, *Rev. Scient. Instrum.* **64**(10), 2947–2951 (1993).
23. R. P. Roy, Stability analysis using two-fluid (SAT) code for boiling flow systems, Electric Power Research Institute Report NP-6103-CCM, Vols 1–4 (1988).
24. N. Zuber and J. A. Findlay, Average volumetric concentration in two-phase flow systems, *ASME J. Heat Transfer* **87,** 453–468 (1965).
25. A. E. Bergles, Instabilities in two-phase systems. In *Two-Phase Flow and Heat Transfer in the Power and Process Industries* (Edited by A. E. Bergles *et al.*), pp. 383–423 (1981).
26. J. March-Leuba, Density-wave instabilites in boiling water reactors, NUREG/CR-6003 and ORNL/TM-12130 (1992).
27. F. C. Moon, *Chaotic Vibrations*. John Wiley, New York (1987).
28. R. T. Lahey, Jr., An application of fractal and chaos theory in the field of two-phase flow and heat transfer, *Wärme- und Stoffübertragung* **26,** 351–363 (1991).
29. R. Seydel, *From Equilbrium to Chaos—Practical Bifurcation and Stability Analysis*. Elsevier, Amsterdam (1988).
30. P. Cvitanović, In *Universality in Chaos* (2nd Edn), pp. 3–34. Adam Higler (1989).